Title

Source signatures from combined isotopic analyses of PM2.5 carbonaceous and nitrogen aerosols at the peri-urban Taehwa Research Forest, South Korea in summer and fall

Authors

Lim, Saehee
Lee, Meehye
Czimczik, Claudia I
et al.

Publication Date

2019-03-01

DOI

10.1016/j.scitotenv.2018.11.157

Peer reviewed

Science of the Total Environment 655 (2019) 1505–1514

Contents lists available at ScienceDirect

Science of the Total Environment

journal homepage: www.elsevier.com/locate/scitotenv

Source signatures from combined isotopic analyses of $PM_{2.5}$ carbonaceous and nitrogen aerosols at the peri-urban Taehwa Research Forest, South Korea in summer and fall

Saehee Lim [a], Meehye Lee [a,*], Claudia I. Czimczik [b,*], Taekyu Joo [a,1], Sandra Holden [b], Gergana Mouteva [b], Guaciara M. Santos [b], Xiaomei Xu [b], Jennifer Walker [b], Saewung Kim [b], Hyun Seok Kim [c,d,e,f], Soyoung Kim [g], Sanguk Lee [g]

[a] Dept. of Earth and environmental sciences, Korea University, Seoul, South Korea
[b] Dept. of Earth System Science, University of California, Irvine, Irvine, USA
[c] Dept. of Forest Sciences, Seoul National University, Seoul, South Korea
[d] Interdisciplinary Program in Agricultural and Forest Meteorology, Seoul National University, Seoul, South Korea
[e] National Center for Agro Meteorology, Seoul, South Korea
[f] Research Institute for Agriculture and Life Sciences, Seoul National University, Seoul, South Korea
[g] National Institute of Environmental Research, Incheon, South Korea

HIGHLIGHTS

- For $PM_{2.5}$, the average $\delta^{13}C$ of TC and $\delta^{15}N$ of TN were -25.4 ± 0.7‰ and 14.6 ± 3.8‰respectively.
- EC and TC were dominated by fossil-fuel (78 ± 7%) and contemporary (76 ± 7%) sources, respectively.
- Low $\delta^{15}N$ (7.0 ± 0.2‰) with high TN concentration was evident in air masses from Shandong province.
- Multi-isotopic composition is useful to trace regional sources of $PM_{2.5}$ aerosol.

GRAPHICAL ABSTRACT

$\delta^{13}C$ of TC versus f_M (EC) for different levels of $\delta^{15}N$ of TN observed at Taehwa Research Forest (TRF) and Gosan Climate Observatory (GCO). TRF samples were classified into groups according to air mass origin.

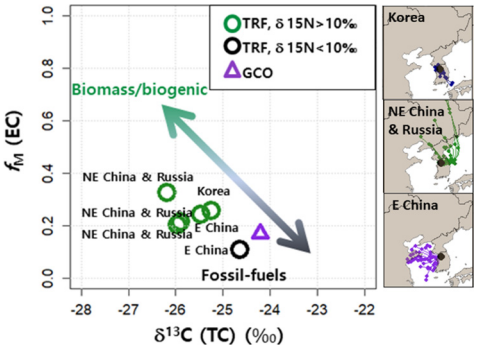

ARTICLE INFO

Article history:
Received 14 July 2018
Received in revised form 8 November 2018
Accepted 10 November 2018
Available online 13 November 2018

Editor: Jianmin Chen

Keywords:
Stable isotope
^{14}C

ABSTRACT

Isotopes are essential tools to apportion major sources of aerosols. We measured the radiocarbon, stable carbon, and stable nitrogen isotopic composition of $PM_{2.5}$ at Taehwa Research Forest (TRF) near Seoul Metropolitan Area (SMA) during August–October 2014. $PM_{2.5}$, TC, and TN concentrations were 19.4 ± 10.1 μg m^{-3}, 2.6 ± 0.8 μg C m^{-3}, and 1.4 ± 1.4 μg N m^{-3}, respectively. The $\delta^{13}C$ of TC and the $\delta^{15}N$ of TN were -25.4 ± 0.7‰ and 14.6 ± 3.8‰, respectively. EC was dominated by fossil-fuel sources with F_{ff} (EC) of 78 ± 7%. In contrast, contemporary sources were dominant for TC with F_c (TC) of 76 ± 7%, revealing the significant contribution of contemporary sources to OC during the growing season. The isotopic signature carries more detailed information on sources depending on air mass trajectories. The urban influence was dominant under stagnant condition, which was in reasonable agreement with the estimated $\delta^{15}N$ of NH_4^+. The low $\delta^{15}N$ (7.0 ± 0.2‰) with high TN concentration was apparent in air masses from Shandong province, indicating fossil fuel combustion as major

* Corresponding authors.
E-mail addresses: meehye@korea.ac.kr (M. Lee), czimczik@uci.edu (C.I. Czimczik).
[1] Now at: School of Earth and Atmospheric Sciences, Georgia Institute of Technology, Atlanta, GA, USA.

https://doi.org/10.1016/j.scitotenv.2018.11.157
0048-9697/

^{13}C
^{15}N
Taehwa Research Forest

emission source. In contrast, the high $\delta^{15}N$ (16.1 ± 3.2‰) with enhanced TC/TN ratio reveals the impact of biomass burning in the air transported from the far eastern border region of China and Russia. Our findings highlight that the multi-isotopic composition is a useful tool to identify emission sources and to trace regional sources of carbonaceous and nitrogen aerosols.

1. Introduction

As a major component (20%–90%) of airborne fine particulate matter ($PM_{2.5}$), carbonaceous aerosol affects health and climate and contributes to low visibility (Pöschl, 2005; Ramanathan and Carmichael, 2008; Jimenez et al., 2009). They exist as a continuum of particles, from light-scattering organic carbon (OC) to light-absorbing brown carbon and highly condensed, light-absorbing elemental (or black) carbon (EC or BC) (Pöschl, 2005; Andreae and Gelencsér, 2006). OC can be directly emitted or originates from the condensation/oxidation of gases (Kanakidou et al., 2005). EC is emitted during incomplete combustion of hydrocarbons, e.g., from coal-firing plants, diesel engines, crop residue burning, and fires (Bond et al., 2013).

In East Asia, aerosols arise from complex anthropogenic and natural sources that vary seasonally (Kim et al., 2007; Streets, 2003; Streets et al., 2009). In summer, aerosol optical depth (AOD) is greatest due to accumulation of pollutants and hygroscopic growth of aerosol in the extended boundary layer (Kim et al., 2007). The mass fraction of secondary aerosols, e.g., sulfate, ammonium, and secondary organic aerosol (SOA), is enhanced in summer (Lim et al., 2012; Zhao et al., 2013). Due to increased emissions mostly from heating, the mass concentrations of $PM_{2.5}$, OC, and EC are greatest in winter (Du et al., 2014; Lim et al., 2012; Ye, 2003) Transboundary air pollution across East Asia is prevalent in winter but also occurs in warm season (Kim et al., 2005; Lim et al., 2012). When the emissions from fossil-fuel combustion is reduced in summer, the crop residue burning is pervasive in China and recognized as a main culprit of summer haze (Chen et al., 2017). Recently, inorganic nitrogen species such as nitrate and ammonium as well as sulfate have been identified as ones of the main contributors developing severe haze events in urban areas of China (Pan et al., 2016; Shang et al., 2018; Yang et al., 2012).

Radiocarbon (^{14}C) is a powerful tool to determine the contribution of fossil and non-fossil sources to carbonaceous aerosols. Fossil-fuel is the predominant source of EC and accounts for ~80% EC emissions in East Asia (Chen et al., 2013; Zhang et al., 2015a; Zhang et al., 2016). It is much less for OC and more than the half of the OC originates from non-fossil sources such as biogenic emissions and biomass combustion (Zhang et al., 2015a; Zhang et al., 2016). Because, these studies have focused on winter season, they reported higher contribution of fossil fuel combustion.

In the warm season of plant growth, the interaction of anthropogenic pollutants (i.e., NO_x, and SO_2) with biogenic organic compounds (e.g., monoterpenes or isoprene) can lead to unexpectedly high formation rates of secondary aerosol (Shilling et al., 2013; Weber et al., 2007; Ying et al., 2014). It is especially of concern in Korea where 70% of the land surface is mountainous and covered by temperate forest. In major urban regions like Seoul metropolitan area (SMA), parks and green area has been increasing, making it imperative to investigate the impact of the biogenic emissions on air quality (Gil et al., 2018).

Stable isotopes of carbon ($\delta^{13}C$) and nitrogen ($\delta^{15}N$) have been used to trace sources and atmospheric process (Aggarwal and Kawamura, 2008; Kirillova et al., 2014; Kundu et al., 2010). Previous studies illustrate that the $\delta^{13}C$ of TC is often between −27‰ and − 21‰, showing the mixed signature of plants, vegetation combustion, and anthropogenic combustion (e.g., Jung and Kawamura, 2011; Kirillova et al., 2014; Pavuluri et al., 2015; Widory, 2006). Particularly in East Asia, $\delta^{13}C$ has been used to trace both anthropogenic and biogenic aerosols transported over long distance (Jung and Kawamura, 2011; Kundu and Kawamura, 2014; Kunwar et al., 2016). Together with the use of organic molecular tracers, it provides further information on atmospheric processing of carbonaceous aerosols (Aggarwal et al., 2013; Aggarwal and Kawamura, 2008; Kawamura et al., 2004). The $\delta^{15}N$ of TN is in wider range from −15 up to ~30‰, resulting from different seasonal and regional emission strength of two main species, NO_3^- and NH_4^+ and their chemistry (e.g., Freyer, 1991; Kawashima and Kurahashi, 2011; Kundu et al., 2010; Widory, 2007). Therefore, the $\delta^{15}N$ along with air mass trajectories could provide constraints for geographically varying emission sources and chemical processes of nitrogen species (Kundu et al., 2010; Pan et al., 2016; Wang et al., 2017).

Here, we characterize the chemical composition of $PM_{2.5}$ at Taehwa Research Forest (TRF) to evaluate the source of air pollution in SMA during summer and fall. Specifically, we quantify $PM_{2.5}$ carbon and nitrogen elemental and isotopic compositions and investigate their emission sources and formation mechanisms.

2. Methods

2.1. Site description

The TRF (37.30°N, 127.32°E, 162 m a.s.l.; shown in Fig. 2) is located about 45 km south of Seoul in Korea. It was established to examine the interaction of anthropogenic and biogenic gases and its effect on ozone and aerosols in SMA (Gil et al., 2018; Kim et al., 2015a, 2015b). The study region is under the influence of the East Asian Monsoon and therefore, subject to seasonal changes in meteorological conditions (Kim et al., 2007). Summer monsoon typically starts with heavy rains in the end of June, during which southerly wind is prevalent under the Pacific High until September. The northerly wind is dominant under the Siberian High during December to February.

To characterize the aerosol burden at TRF in the regional and seasonal context, we additionally collected $PM_{2.5}$ at Gosan Climate Observatory (GCO) on Jeju Island and over the Yellow Sea (Fig. 2). GCO is a background site (33.17°N; 126.10°E; 1000 m a.s.l.) of East Asia, being served as one of the Asian Brown Cloud (ABC) superstations (Lee et al., 2007), and the aerosol characteristics of GCO have been well-documented in previous studies (e.g., Kim et al., 2007; Lim et al., 2012, 2014).

2.2. Aerosol sampling

$PM_{2.5}$ aerosol was sampled at TRF (n = 17) during the summer and fall of 2014 (August 13 to October 23) (Table 1 and Fig. 1). A high-volume aerosol sampler (HIVOL-AMCLD, Thermo Environmental Instruments, Franklin, MA, USA) with a $PM_{2.5}$ impactor plate (TE-230-QZ, Tisch Environmental, Cleves, OH, USA) was installed on the upper level of a container (about 6 m above the ground). A slotted micro-quartz fiber filter (TE-230-QZ, Tisch) was installed in the high-volume impactor head to filter out particles >2.5 μm diameter. Samples were collected mostly for 2–3 days (Table 1), on 20 cm × 25 cm quartz fiber filters (2500 QAT-UP, Pallflex Tissuquartz, Pall, Port Washington, NY, USA). A blank filter (one-fourth of the sample filter) was mounted inside of the aerosol sampler housing. Filters were wrapped in aluminum foil and pre-baked at 500 °C for 4 h. After sampling, filters were transported on ice packs to the lab and stored in freezer. In addition, we obtained daily $PM_{2.5}$ sample for mass using a sharp-cut cyclone. At GCO, a $PM_{2.5}$ sample was collected on a pre-baked quartz filter for 8 days using a high-volume sampler (DH77, Digitel A.G., Switzerland)

Table 1
Overview of elemental and isotopic composition of $PM_{2.5}$ measured at Taehwa Research Forest (TRF) and Gosan Climate Observatory (GCO) and over the Yellow Sea in 2014.

Sample ID	Start	End	$PM_{2.5}$	f_M (TC)[c]	F_c (TC)	TC	TN	TC/TN	$\delta^{13}C$ (TC)	$\delta^{15}N$ (TN)	f_M (EC)[c]	F_{ff} (EC)	OC/EC[d]	Air mass[e]
	MM/DD/YY Hour:Min		$\mu g\ m^{-3}$		%	$\mu g\ m^{-3}$			‰			%		
Taehwa (TRF)														
T1	8/13/14 11:31	8/14/14 14:17	27.0	0.7382 (0.0019)	72	2.27	2.34	1.0	−25.4	15.6	n.m.	n.m.	13.8	Korea
T2	8/15/14 10:47	8/17/14 10:48	25.9	2.0872 (0.0034)	n.r.	3.75	1.49	2.5	−25.3	16.3	0.2559 (0.0297)	75	8.0	Korea
T3	8/22/14 10:48	8/24/14 10:47	48.6	0.8608 (0.0015)	84	3.36	6.45	0.5	−24.9	7.1	0.1070 (0.0507)	90	10.4	E China
T4	8/26/14 10:49	8/28/14 9:49	11.2	0.7716 (0.0014)	75	1.15	0.21	5.5	−26.4	10.6	n.m.	n.m.	14.3	Marine
T5	8/28/14 10:45	9/1/14 10:50	15.2	1.0915 (0.0018)	n.r.	2.47	0.66	3.7	−26.0	18.5	0.2027 (0.0366)	80	12.5	NE China & Russia
T6	9/1/14 11:06	9/2/14 15:09	15.1	1.6345 (0.0034)	n.r.	3.26	0.94	3.5	−26.0	16.7	n.m.	n.m.	10.1	NE China & Russia
T7	9/12/14 10:55	9/15/14 10:35	12.0	0.7757 (0.0013)	75	2.33	0.90	2.6	−26.0	18.6	0.2118 (0.0391)	79	8.8	NE China & Russia
T8	9/15/14 10:50	9/17/14 10:35	22.1	1.2457 (0.0020)	n.r.	4.25	1.30	3.3	−25.7	13.6	0.2413 (0.0429)	77	12.3	E China
T9	9/17/14 10:50	9/19/14 10:20	21.3	1.5294 (0.0029)	n.r.	2.42	0.77	3.1	−26.3	16.3	0.3233 (0.0320)	69	5.1	NE China & Russia
T10	9/19/14 10:40	9/22/14 10:48	26.5	0.7989 (0.0012)	78	2.96	1.12	2.6	−25.7	15.3	n.a.	n.a.	n.a.	Korea
T11	9/22/14 10:48	9/23/14 10:22	25.2	0.6991 (0.0013)	68	2.56	1.21	2.1	n.r.	14.3	n.a.	n.a.	n.a.	E China
T12	9/25/14 10:45	9/27/14 10:34	10.4	0.6658 (0.0013)	65	2.13	0.85	2.5	−26.0	16.2	n.a.	n.a.	n.a.	E China
T13	9/27/14[a] 10:55	9/30/14 10:15	21.2	1.1032 (0.0017)	n.r.	2.24	2.73	0.8	−24.0	6.9	n.a.	n.a.	n.a.	E China
T14	9/30/14 10:15	10/4/14 10:55	20.3	0.9369 (0.0018)	91	2.24	1.16	1.9	−24.3	16.9	n.a.	n.a.	n.a.	Mixed
T15	10/4/14 10:55	10/6/14 11:48	6.4	0.8227 (0.0015)	80	1.58	0.66	2.4	−25.8	10.7	n.a.	n.a.	n.a.	NE China & Russia
T16	10/6/14[b] 12:05	10/13/14 10:28	11.9	0.7785 (0.0012)	76	3.37	1.04	3.2	−24.7	15.6	n.a.	n.a.	n.a.	Mixed
T17	10/13/14[b] 10:50	10/23/14 11:35	9.1	0.7922 (0.0012)	77	2.52	0.46	5.5	−24.8	19.9	n.a.	n.a.	n.a.	Mixed
Gosan (GCO)														
G1	6/11/14 0:00	6/19/14 0:00	n.m.	0.6139 (0.0021)	60	5.4	5.08	1.1	−24.2	14.9.	0.1687 (0.0184)	84	9.7	70% westerly & 30% easterly
Yellow Sea (Gisang 1)														
Y1	11/18/14 9:30	11/18/14 17:22	n.m.	0.6774 (0.0018)	66	n.r.	n.r.	n.r.	n.r.	n.r.	n.a.	n.a.	n.a.	Predominantly westerly
Y2	11/22/14 16:27	11/23/14 17:45	n.m.	0.5086 (0.0012)	49	3.15	2.90	1.1	−24.2	4.4	n.a.	n.a.	n.a.	
Y3	11/23/14 18:36	11/24/14 14:30	n.m.	0.5226 (0.0014)	51	n.r.	1.34	n.r.	n.r	6.1	n.a.	n.a.	n.a.	

n.a. not analyzed, n.r. = not reported, below detection limit or contaminated with extra ^{14}C, n.m. = not measured due to failed graphitization.
[a] Sampling interrupted for 50 min.
[b] Unstable flow, minimum load estimates.
[c] Radiocarbon content expressed as fraction modern, mean (2σ).
[d] Calculated as (bulk C-EC)/EC, with EC determined with the Swiss_4S protocol.
[e] Hysplit 2-day backward air-mass trajectories calculated at four-hourly intervals for each sampling period.

during June 11–14 of 2014 (Table 1). Over the Yellow Sea, three $PM_{2.5}$ samples were collected for 8–25 h using a high-volume sampler (HIVOL-AMCLD, Thermo) onboard the R/V Gisang 12 m above the sea surface during November 18–24 of 2014. The filters were prepared and stored in the same way as the TRF filters.

2.3. Analytical methods

2.3.1. Isotopes for bulk $PM_{2.5}$

All samples from TRF, GCO, and the Yellow Sea were analyzed at UC Irvine for their total carbon (TC) and total nitrogen (TN) concentrations and stable isotopic contents. Based on the bulk filter color of light gray, dark gray, and charcoal, one or two 1.5 cm^2 pieces were cut out with a sample punch (SP-15, 1 cm × 1.5 cm, Sunset Laboratory, Portland, OR, USA), weighed into tin capsules (5 mm × 9 mm, 041077, Costech Analytical Technologies, Valencia, CA, USA), and analyzed with an elemental analyzer (EA, Fisons NA-1500NC, Thermo, Waltham, MA, USA) coupled with an isotope-ratio mass spectrometer (IRMS, DeltaPlus XL, Thermo). Samples were analyzed alongside field blanks and analytical standards, and data are reported using conventional delta notation relative to V-PDB for $\delta^{13}C$ and to AIR for $\delta^{15}N$ and corrected for filter field blanks. The measurement uncertainty was 0.1‰ for $\delta^{13}C$ and 0.2‰ for $\delta^{15}N$ (1σ, from long-term measurements of secondary standards).

All bulk samples were also analyzed for their ^{14}C content. Multiple punches (n = 3–25 based on TC content) were sealed with 80 mg of cupric oxide under vacuum in pre-combusted 9-mm-o.d. quartz tubes and combusted at 900 °C for 3 h. For each location, we also analyzed one composite field blank (23–80 punches per site). The resulting sample or blank CO_2 was purified cryogenically on a vacuum line and reduced

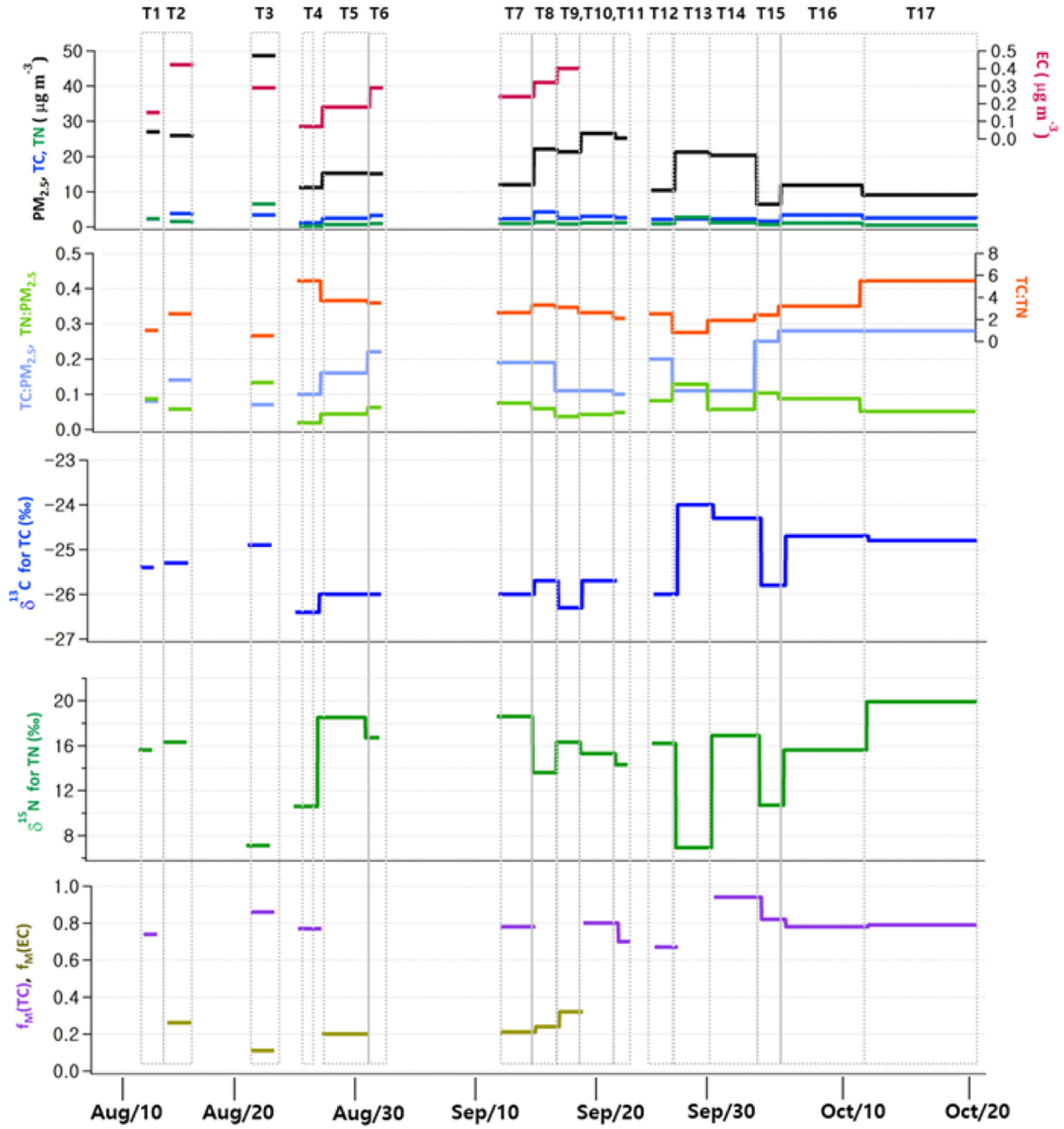

Fig. 1. Time series of the chemical composition of $PM_{2.5}$ at Taehwa Research Forest (TRF) in summer and fall of 2014. Each sampling period is indicated by a gray box with a label at the top.

to graphite using a sealed-tube zinc reaction technique (Xu et al., 2007). The graphite was analyzed alongside graphitization standards and blanks by the accelerator mass spectrometry (AMS, NEC 0.5 MV 1.5SDH-1, National Electrostatics Corporation, Middleton, WI, USA) at the W. M. Keck Carbon Cycle AMS facility at UC Irvine (Beverly et al., 2010). Data are reported as fraction modern (f_M), with ^{13}C fractionation correction using on-line AMS $^{13}C/^{12}C$, following the conventions of Stuiver and Polach. The uncertainty is about 2–3‰ for modern samples (1σ, from long-term measurements of secondary standards). For samples with >0.3 mg C, a fraction of the CO_2 was split and also analyzed for its stable TC isotopic composition on a GasBench (Thermo) coupled with an isotope mass ratio spectrometer (IRMS; DeltaPlus XL, Thermo). For bulk $PM_{2.5}$ analyzed with both EA-IRMS (see above, n = 1–2 punches/sample) and GasBench-IRMS (n = 3–25 punches/sample), we reported the average $\delta^{13}C$ data (Table 1) weighted according to the number of filter punches used in each method.

2.3.2. Isotopes for elemental carbon (EC) and organic carbon (OC)

A subset of samples from TRF (n = 6) and a sample from GCO were also analyzed for the ^{14}C content of EC. A 2.5 cm^2 filter punch was washed with 20 mL MilliQ H_2O using a syringe filter (UX-29550-42, Cole-Parmer, Vernon Hills, IL, USA) to remove water-soluble OC to prevent charring; this was followed by oven-drying at 60 °C. Then, EC was isolated from a 1.5 cm^2 filter punch taken from the center of the 2.5 cm^2 punch. The EC was oxidized to CO_2 with a thermal-optical OC/EC analyzer (Sunset) following the SWISS_4S protocol (Zhang et al., 2012). The EC-CO_2 was purified cryogenically and quantified manometrically on a vacuum line (Mouteva et al., 2015). Finally, the EC-CO_2 was converted to graphite using a hydrogen reduction method adapted for ultra-small samples (Santos et al., 2007) and measured using AMS as described for the bulk samples. The samples were processed alongside procedure blanks and standards; the processing uncertainty was 2 μg C (Mouteva et al., 2015).

The OC concentrations were calculated as the difference between TC and EC, and the ^{14}C content of the OC was estimated using the isotope mass balance:

$$f_M\,(OC) = \{TC \times f_M\,(TC) - EC \times f_M\,(EC)\}/OC \quad (1)$$

Within the OC–EC aerosol continuum, the Swiss_4S protocol disregards a middle fraction to minimize the risk of charring (Zhang et al., 2012), which can transfer OC-derived carbon into the EC fraction and affect its ^{14}C content. Compared to other approaches, our protocol may therefore underestimate the size of the EC fraction and overestimate the size of the OC fraction.

2.3.3. Source apportionment of total carbon (TC) and EC

The f_M values of TC and EC can be used to estimate the contributions of contemporary (non-fossil) vs. fossil-fuel sources. The fractions (%) of contemporary (F_c (TC)) and fossil-fuel combustion (F_{ff} (TC)) sources to TC were estimated as

$$\mathrm{Fc}\ (\mathrm{TC}) = \frac{f_M(TC) - f_M(ff)}{f_M(c) - f_M(ff)} \times 100 \quad (2)$$

$$\mathrm{Fff}\ (\mathrm{TC}) = \frac{f_M(TC) - f_M(c)}{f_M(ff) - f_M(c)} \times 100 \quad (3)$$

where f_M (c) and f_M (ff) indicate the f_M values of contemporary and fossil-fuel combustion emissions, respectively. For f_M (c), the mean f_M (c) of $^{14}CO_2$ (1.0289) was adopted, which was measured at Pt. Barrow, Alaska during June–September 2014 (X. Xu pers. com. 2018). The f_M (ff) is approximated as 0. The source apportionment of EC was further estimated following the Eqs. (2) and (3).

2.3.4. Backward trajectory analysis

For each sample, air mass trajectories were traced backward at 1000 m a.g.l. using the HYSPLIT model with meteorological input from the global data assimilation system (GDAS) (Stein et al., 2015; http://ready.arl.noaa.gov) (Fig. 2). Trajectories were calculated at 00:00 UTC every 4 h for 48 h at TRF and for 72 h at GCO. For GCO, two-thirds of sampling period was influenced by air masses from East China and one-third from the East China Sea, the Pacific, and Japan (Fig. S1). Over the Yellow Sea, the westerly condition was dominant in November (Kim et al., 2007).

3. Results and discussion

3.1. $PM_{2.5}$ TC and total nitrogen (TN) mass concentrations

Throughout the sampling period, $PM_{2.5}$ concentration ranged from 6.4 to 48.6 μg m^{-3} with the mean of 19.4 ± 10.1 μg m^{-3} (1σ SD) (Table 1 and Fig.1). While TC concentration varied from 1.2 to 4.3 μg C m^{-3} with the mean of 2.6 ± 0.8 μg C m^{-3}, TN concentration ranged from 0.2 to 6.5 μg N m^{-3} with the mean of 1.4 ± 1.4 μg N m^{-3}. TC and TN accounted for 16% and 7% of $PM_{2.5}$ mass on average, respectively, and the mean TC/TN ratio was 2.8 ± 1.4. Among these, the $PM_{2.5}$ mass and TC concentrations were slightly lower than those measured at an urban site in Seoul for the same period, which were 22.1 ± 19.3 μg m^{-3} and 3.0 ± 2.2 μg C m^{-3}, respectively (NIER, 2014). Given the location of TRF adjacent to the SMA, this result implies the TRF was subject to the urban influence.

3.2. $\delta^{13}C$ and f_M for TC

The $\delta^{13}C$ of TC was −25.4 ± 0.7‰ at TRF. Considering the high OC/EC ratio of 10.6 ± 3.0 (Table 1), the observed $\delta^{13}C$ values were subject to a greater contribution of OC. The $\delta^{13}C$ was comparable to those of GCO (−24.2‰; n = 1) and the Yellow Sea (−24.2‰; n = 1) (Table 1) and those observed across Asia including Beijing and India (Aggarwal et al., 2013; Kawamura et al., 2004; Schleicher et al., 2013). The $\delta^{13}C$ values of the three sites indicate a wide range of carbon emission sources, e.g., biogenic emissions, anthropogenic combustion of liquid fuels (gasoline, diesel, and fuel oil), and combustion of C3-dominated vegetation (Turekian et al., 1998a; Widory et al., 2004; Widory, 2006; Fisseha et al., 2009). Therefore, the $\delta^{13}C$ values of the present study likely reflect the typical emission sources of carbonaceous aerosol on a regional scale.

Most samples were depleted in ^{14}C with a f_M (TC) of 0.79 ± 0.07 (mean ± 1σ SD, n = 11), excepting six samples enriched in ^{14}C with f_M (TC) = 1.09–2.09, which were much higher than the atmospheric $^{14}CO_2$ level since 1950 (Graven, 2015). Such highly elevated ^{14}C-$PM_{2.5}$ (Buchholz et al., 2013) and $^{14}CO_2$ (Trumbore et al., 2002) above the background level have previously been observed in other urban and rural areas and is typically attributed to intermittent combustion of ^{14}C-enriched waste. The highest f_M was detected during August 15–17 under highly stagnant condition. Thus, it is likely due to the local contamination of ^{14}C from medical waste incineration in SMA. For the other five samples with f_M between 1.1 and 1.6, air masses traveled relatively a long distance from North Korea. From swipe test, it was confirmed that there was no trace for ^{14}C contamination in the measurement process from the sampling to the chemical analysis. Therefore, these six samples with f_M of TC ≥ 1.09 were excluded in the following discussion. Non-contaminated TRF samples ranged from 65 to 91% of the contemporary sources of TC (F_c (TC)) with a mean of 76 ± 7%. The F_c (TC) was greater than that of GCO (60%; n = 1) and over the Yellow Sea (49–66%; n = 3) (Table 1). The F_c (TC) of TRF was even higher than those of urban background sites on a global scale (40%–60%; Heal, 2014, and references therein).

3.3. f_M for EC and OC

EC was dominated by fossil-fuel sources (F_{ff} (EC); n = 6) with a mean contribution of 78 ± 7%. This fossil-fuel contribution was similar to that of GCO with F_{ff} (EC) of 84% in the present study (n = 1) and of 76 ± 11% on annual average in the previous study (Zhang et al., 2016). The F_{ff} (EC) of TRF is comparable to the annual mean of Beijing (79% ± 6%; Zhang et al., 2015b), the winter fraction of Beijing (76 ± 4%; Zhang et al., 2015a) and Shanghai (79 ± 4%; Zhang et al., 2015a), and the annual mean of a European background site (~80%; Dusek et al., 2017). Like these sites, fossil-fuel combustion would be a major source of EC burden for TRF. In the previous study, vehicle emissions from nearby roads have been identified as main sources for EC at TRF (Ham et al., 2016). In contrast, OC was dominated by contemporary sources with F_c (OC) of 89 ± 7% (n = 2), albeit the small number of samples (n = 2). It is likely to be the result of the photo-oxidation of biogenic VOCs (BVOCs) leading to the local production of OC at TRF particularly in growing season (Kim et al., 2015a, 2015b).

3.4. $\delta^{15}N$ for TN

All TRF samples were enriched in ^{15}N with a mean $\delta^{15}N$ of 14.6 ± 3.8‰, which was higher than that of the Yellow Sea (5.3 ± 1.2‰; n = 2) (Fig. 3). The heavier ^{15}N isotope is enriched in secondary aerosol because of fractionation during gas-to-particle conversion (Heaton, 1987). The TRF $\delta^{15}N$ of TN is rather similar to those of GCO in summer and fall (~16‰) (Kundu et al., 2010) and a mountain site of northeast China in early fall (18‰) (Wang et al., 2017). The secondary nitrogen aerosol comprises mainly NO_3^- and NH_4^+. In East Asia, the reported $\delta^{15}N$ of NH_4^+ was consistently high particularly in summer and fall as approximately 20‰ (Kawashima and Kurahashi, 2011; Kundu et al., 2010), and the $\delta^{15}N$ of NO_3^- was often close to ~0‰ (Kawashima and Kurahashi, 2011).

In summer, the average NOx was low at TRF (Ham et al., 2016) as well as China (Wang et al., 2007). In contrast, NH_3 levels were the

highest across China (Pan et al., 2018). At TRF, the mean mass ratio of NH_4^+-N/NO_3^--N was higher in August (9.3) than in June (3.8) (NIER, 2013). Under high atmospheric NH_3 level, the isotopic equilibrium of $NH_3 \Leftrightarrow NH_4^+$ results in ^{15}N enrichment in particle-phase. In contrast, the isotopic fractionation factor between NOx and NO_3^- is small (Freyer, 1991; Yeatman et al., 2001). The source fingerprint of $\delta^{15}N$ varies in a wide range. For example, the $\delta^{15}N$-NOx is less than −10‰ for biogenic NOx from bacteria, from −20 to 10 for vehicle NOx, and from 5 to 20‰ for power plant NOx (Felix et al., 2012; Felix and Elliott, 2014; Heaton, 1990; Walters et al., 2015). The $\delta^{15}N$-NH_3 ranges from −55 to −25‰ for livestock waste and fertilizer, −15 to −11‰ for power plant, and − 17 to −2‰ for vehicle exhaust (Chang et al., 2016; Felix et al., 2013). The $\delta^{15}N$ of TN is from −20 to 3 for fuel oil, from 3 to 15 for natural gas (Widory, 2007; Widory et al., 2004), and about 20‰ for biomass burning (Kundu et al., 2010; Turekian et al., 1998). Taken together, the $\delta^{15}N$ values of TRF thus indicate that during growing season, the equilibrium fractionation of $NH_3 \Leftrightarrow NH_4^+$ was likely more responsible for observed $\delta^{15}N$ of TN than the conversion of NO_x to NO_3^-. In particular, the high $\delta^{15}N$ implies that the secondary formation of NH_4^+ played a major role in nitrogen constituents of $PM_{2.5}$.

3.5. Isotopic signature of different air masses

Carbon sources were apportioned using the ^{14}C-based approach: EC was dominated by fossil-fuel sources and OC by biogenic sources. The $\delta^{15}N$ shows relatively larger variability than the $\delta^{13}C$ values (Table 1 and Fig. 3), which should be associated with secondary nitrogen aerosol formation as well as various emission sources of nitrogen species. Here, we further categorize the TRF samples according to air mass type based on backward air-mass trajectories (Fig. 2) in order to relate the isotopic composition of $PM_{2.5}$ to the geographical origins, focusing on emission sources and formation of nitrogen species.

During August–October 2014, the air masses arriving at TRF originated from four source regions: Northeast China and Russia (hereafter, NE China & Russia), Marine, the Korean Peninsula (Korea), and East China (E China) (Fig. 2). These four groups were distinctive in mass, composition, and isotopic signature, particularly in $\delta^{15}N$. For three $PM_{2.5}$ samples collected for longer period (Table 1), air masses were mixed and their isotopic signature was not clearly distinguished (Table 2 and Fig. 4).

3.5.1. Marine and NE China & Russia

When the air came from the East Sea, the mean concentrations of $PM_{2.5}$, TC and TN were the lowest but the TC/TN ratio was the highest among the four groups (Fig. 2a). It was classified as marine air, representing the seasonal background. More often, air was transported through the East Sea from the eastern border region of China and Russia. For this NE China & Russia air (Fig. 2c), the $PM_{2.5}$ and TN concentrations were lower than those of Korea and E China air by ~54% and 38%, with comparable TC levels.

The mean $\delta^{15}N$ of 10.6‰ for marine air was generally lower than those of other groups (Fig. 4b). Although the number of samples is

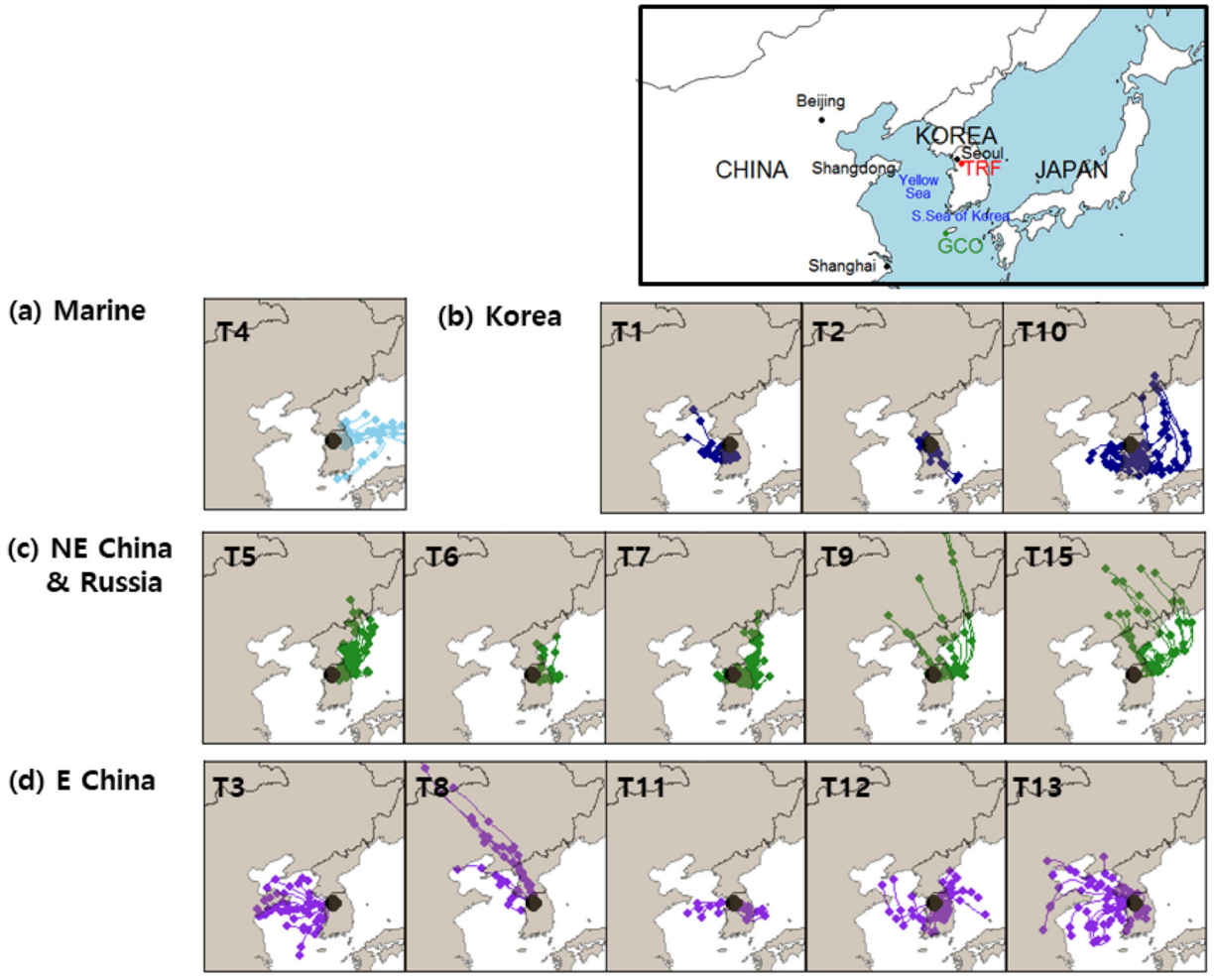

Fig. 2. Categorized two-day backward air-mass trajectories calculated with the HYSPLIT model starting at TRF (37.30°N; 127.32°E; 1000 m a.s.l.) using GDAS meteorological data. The trajectories were calculated every 4 h. A map of East Asia with our sampling sites (red: TRF, blue: Yellow Sea, green: GCO) is shown on the top right. Mixed air masses are not shown.

Table 2
Summary of $PM_{2.5}$ elemental and isotopic composition in various air masses arriving at TRF. Data are reported as mean (1σ).

Air mass origin	n	$PM_{2.5}$	TC	TN	TC:TN	$\delta^{13}C$ (TC)	$\delta^{15}N$ (TN)	f_M (TC)	f_M (EC)
		μg m^{-3}	μg m^{-3}			‰			
Marine	1	11.2	1.2	0.2	5.5	−26.4	10.6	0.7716 (0.0014)	n.m.
NE China & Russia	5	14.0 (5.4)	2.4 (0.6)	0.8 (0.1)	3.1 (0.6)	−26.0 (0.2)	16.1 (3.2)	0.7992 (0.0332)	0.2459[a] (0.0672)
Korea	3	26.5 (0.5)	3.0 (0.7)	1.7 (0.6)	2.0 (0.9)	−25.4 (0.2)	15.7 (0.5)	0.7686 (0.0429)	0. 2559[b] (0.0297)
E China	5	25.5 (14.1)	3.0 (0.9)	2.5 (2.3)	1.8 (1.2)	−25.2 (0.9)	11.6 (4.3)	0.7419 (0.1043)	0.1742[c] (0.0950)
Mixed	3	13.8 (5.95)	2.7 (0.69)	0.9 (0.4)	3.6 (1.8)	−24.6 (0.3)	17.5 (2.2)	0.8359 (0.0878)	n.m.

n.m. = not measured.
[a] n = 3.
[b] n = 1.
[c] n = 2.

small, the lower $\delta^{15}N$ value may reflect an oceanic source of NH_3 (Quinn et al., 1988; Yeatman et al., 2001). In addition, the increased scavenging time due to long-range transport may be responsible for the lower $\delta^{15}N$ value in marine air. In NE China & Russia air, the isotopic signature was slightly higher in $\delta^{15}N$ (16.1 ± 3.2‰) and f_M (TC) (0.80 ± 0.03) and depleted in $\delta^{13}C$ (−26.0 ± 0.2‰) together with the relatively higher TC/TN ratio. It indicates that the air mass was influenced by biomass burning (e.g., C3 plant combustion) (Turekian et al., 1998; Kundu et al., 2010) probably transported from the northeast China and Russia. In summer and fall, crop residue burning and second-season rice straw burning are prevalent in China (Chen et al., 2017, and references therein) and wildfires in the Russian Far East (e.g., Kawano and Komatsu, 2012). Indeed, Kundu et al. (2010) reported relatively high $\delta^{15}N$ of TN in East Asian outflows (~16–17‰ at GCO) during summer and fall.

3.5.2. Korea

The highest $PM_{2.5}$, TC, and TN concentrations were observed in Korea and E China air masses. The Korea air represents the influence of urban emissions from SMA under stagnant atmospheric conditions (Fig. 2b). $PM_{2.5}$ and TC were 2.5 times higher and TN was 7 times higher than those of Marine air (Table 2 and Fig. 4a). For the two samples (T1 for August 13–14 and T2 for August 15–17) that were collected under severely stagnant condition, the estimation of $\delta^{15}N$-NH_3 was attempted, assuming the vehicle source for NO_3^- ($\delta^{15}N$-NO_x from Walters et al., 2015) and the isotope exchange equilibrium with the isotope enrichment factor of +33‰ between NH_3 and NH_4^+ (Heaton et al., 1997). With the NH_4^+-N/NO_3^--N ratio of 10 that was measured in August from the previous study (NIER, 2013), the $\delta^{15}N$-NH_3 was estimated to be −16‰ to −13‰. This value most likely indicates the source for vehicle exhaust, livestock waste, and power plant (Chang et al., 2016; Felix et al., 2013), which is plausible under stagnant condition during summer. (See Fig. 2b.)

3.5.3. E China

E China air was characterized by low TC/TN ratio (1.8 ± 1.2), $\delta^{15}N$ (11.6 ± 4.3‰), and f_M (EC) (0.17 ± 0.09). Two samples (T3 for August 22–26 and T13 for September 27–30) were distinguished by the lowest $\delta^{15}N$ (7.0 ± 0.2‰) together with the highest TN mass (4.6 ± 2.6 μg N m^{-3}) (Fig. 4b) and low TC/TN ratio (0.7 ± 0.2) (Fig. 4a). Their $\delta^{15}N$ values were close to the mean $\delta^{15}N$ for the Yellow Sea samples (5.3 ± 1.2‰; Fig. 3), for which the contribution of fossil-fuel source was high (f_M (TC) of 0.57 ± 0.09; Table 1). The isotopic signature of "T3" and "T13", therefore, likely indicates the impact of fossil fuel-

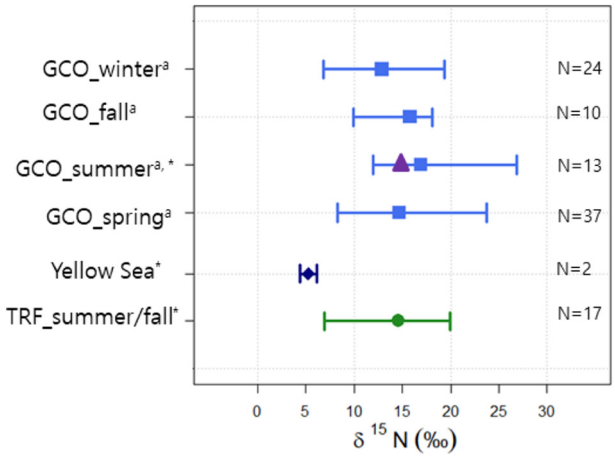

Fig. 3. Ranges of $\delta^{15}N$ values measured at TRF (green), Yellow Sea (dark blue), and GCO (violet).*This study. [a]Seasonal $\delta^{15}N$ values of GCO (sky blue) are from Kundu et al. (2010). Marker indicates mean value at each site and left and right bounds indicate minimum and maximum values, respectively. $\delta^{15}N$ values between TRF and Yellow Sea are significantly different at $p < 0.005$.

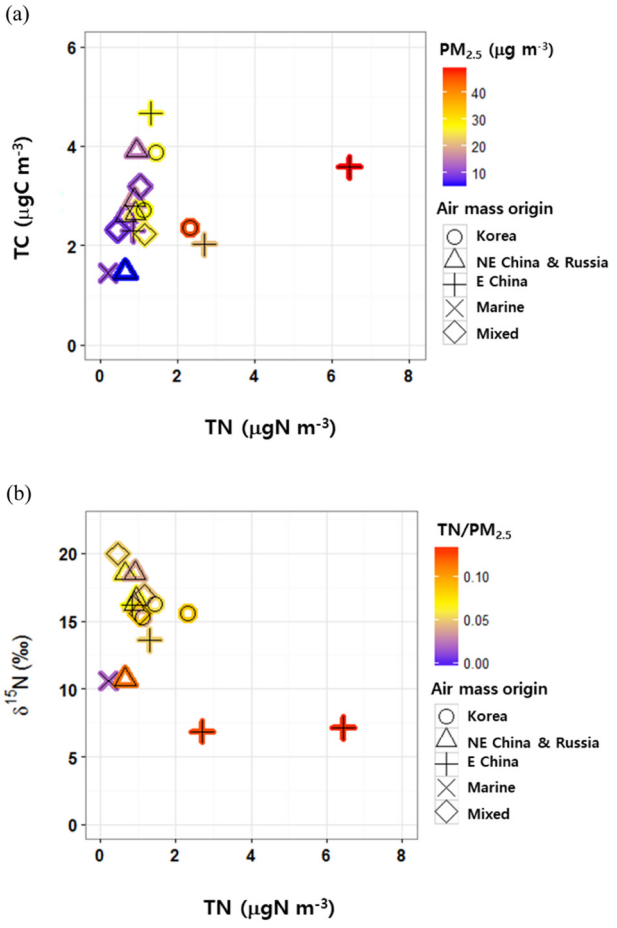

Fig. 4. (a) TN versus TC for $PM_{2.5}$ and (b) TN versus $\delta^{15}N$ for TN/$PM_{2.5}$. Shapes indicate air mass origins.

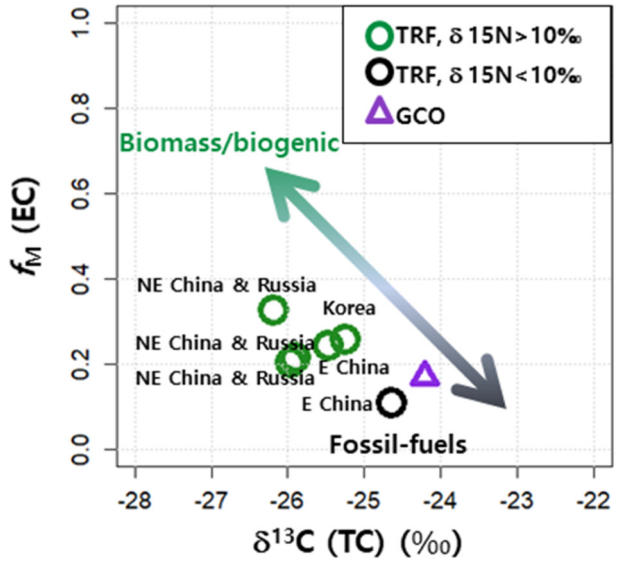

Fig. 5. δ^{13}C of TC versus f_M (EC) for different δ^{15}N values observed at TRF and GCO. TRF samples were classified into groups according to air mass origin.

laden pollution plumes transported from urban China. The combined isotopic signatures correspond to anthropogenic NO_x emissions from industries and vehicles (Felix and Elliott, 2014; Widory, 2007). Precipitation effect was probably negligible on changes in δ^{15}N; the δ^{15}N value for "T3" with a little precipitation was similar to that for "T13" without precipitation.

Back-trajectories show that these two air masses originated from Shandong Province and reached the TRF (Fig. 2d). The isotopic evidence for Shandong Province pollution plumes was further supported by a sharp increase in AOD (at 0.55 μm) in the downwind region of the Yellow Sea and the central Korea surrounding TRF during August 22–26 (corresponding to "T3"; up to 1.9) and September 27–30 (corresponding to "T13"; up to 1.1) (Fig. S2). The higher AOD of these periods also coincided with the lowest f_M (EC) observed in this study (0.11 ± 0.05). This agreement confirms that the isotopic signature is a convincing evidence for regional source identification in Northeast Asia.

3.6. Combined isotopic signature

The isotopic measurements of this study highlight that the multi-isotopic composition including f_M (EC), δ^{13}C, and δ^{15}N is a diagnostic tool to distinguish $PM_{2.5}$ sources in Northeast Asia. In high f_M (EC) and low δ^{13}C domain, δ^{15}N was relatively high and vice versa (Fig. 5). This multiple-isotope approach again reveals that the contribution of fossil-fuel sources to $PM_{2.5}$ was more pronounced in urban China than the downstream region.

4. Conclusions

This study determined the carbon and nitrogen isotopic compositions of $PM_{2.5}$ at Taehwa research forest (TRF) near SMA during August–October 2014. The mean concentrations of $PM_{2.5}$, TC, and TN were 19.4 ± 10.1 μg m^{-3}, 2.6 ± 0.8 μg C m^{-3}, and 1.4 ± 1.4 μg N m^{-3}, respectively. The mean δ^{13}C of TC and δ^{15}N of TN were − 25.4 ± 0.7. δ^{15}N and 14.6 ± 3.8‰, respectively with relatively larger variability in δ^{15}N than δ^{13}C. Fossil-fuel sources accounted for 78 ± 7% of EC. In contrast, TC and OC were dominated by contemporary sources with 76 ± 7% and 89 ± 7%, respectively, showing biogenic carbon as important $PM_{2.5}$ source at the forest site during the growing season.

The isotopic composition showed different characteristics depending on the air mass history. In the air transported from the Far East region, the mean δ^{15}N and f_M (TC) were slightly high as 16.1 ± 3.2‰ and 0.80 ± 0.03 with the low δ^{13}C (−26.0 ± 0.2‰) and relatively high TC/TN ratio, suggesting the impact of biomass burning plumes from northeast China and Russian Far East. Under stagnant condition, the urban influence of Seoul Metropolitan Area (SAM) was evident. Particularly, the estimated δ^{15}N of NH_4^+ implies the anthropogenic sources of vehicle exhaust, livestock waste, and power plant. The low δ^{15}N (7.0 ± 0.2‰) of Shandong province air along with low mean δ^{15}N of the Yellow Sea reflects the aerosol signature of urban China. In the present study, low δ^{15}N together with high TN concentration (4.6 ± 2.6 μg N m^{-3}) was highlighted as an clear evidence for the transport of fossil fuel-laden plumes transported from urban China.

The multiple-isotope composition including f_M (EC), δ^{13}C, and δ^{15}N is especially advantageous for identifying emission sources of carbonaceous and nitrogen aerosols and their regional sources in East Asia. In the warm season, the large contribution of contemporary emissions to OC and NH_4^+ is especially of concern in terms of policy.

Acknowledgments

This research was supported by the National Strategic Project-Fine Particle of the National Research Foundation of Korea (NRF) funded by the Ministry of Science and ICT (MSIT), the Ministry of Environment (ME), and the Ministry of Health and Welfare (MOHW) (2017M3D8A1092015). Funding (to S. Lim) was provided by the Basic Science Research Program of the National Research Foundation of Korea (NRF) and the Ministry of Education (2015R1A6A3A01061393 and 2016R1D1A1B03934532), and (to S. R. Holden) via a U.S. NOAA Climate and Global Change Fellowship. We thank J. Wessling for assistance with sample preparation in the laboratory and the KCCAMS staff, in particular J. Southon, X. Xu, and D. Zhang, for their assistance with sample analyses. We gratefully acknowledge the NOAA Air Resources Laboratory (ARL) for providing the HYSPLIT transport and dispersion model and/or READY website (http://www.ready.noaa.gov) used in this publication. We also acknowledge the MODIS mission scientists and associated NASA personnel for the production of data used in this research effort.

Appendix A. Supplementary data

Supplementary data to this article can be found online at https://doi.org/10.1016/j.scitotenv.2018.11.157.

References

Aggarwal, S.G., Kawamura, K., 2008. Molecular distributions and stable carbon isotopic compositions of dicarboxylic acids and related compounds in aerosols from Sapporo, Japan: implications for photochemical aging during long-range atmospheric transport. J. Geophys. Res. 113, D14301. https://doi.org/10.1029/2007JD009365.

Aggarwal, S.G., Kawamura, K., Umarji, G.S., Tachibana, E., Patil, R.S., Gupta, P.K., 2013. Organic and inorganic markers and stable C-, N-isotopic compositions of tropical coastal aerosols from megacity Mumbai: sources of organic aerosols and atmospheric processing. Atmos. Chem. Phys. 13, 4667–4680. https://doi.org/10.5194/acp-13-4667-2013.

Andreae, M.O., Gelencsér, A., 2006. Black carbon or brown carbon? The nature of light-absorbing carbonaceous aerosols. Atmos. Chem. Phys. 6, 3131–3148. https://doi.org/10.5194/acp-6-3131-2006.

Beverly, R.K., Beaumont, W., Tauz, D., Ormsby, K.M., von Reden, K.F., Santos, G.M., Southon, J.R., 2010. The Keck Carbon Cycle AMS Laboratory, University of California, Irvine: status report. Radiocarbon 52, 301–309. https://doi.org/10.1017/S0033822200045343.

Bond, T.C., Doherty, S.J., Fahey, D.W., Forster, P.M., Berntsen, T., Deangelo, B.J., Flanner, M.G., Ghan, S., Kärcher, B., Koch, D., Kinne, S., Kondo, Y., Quinn, P.K., Sarofim, M.C., Schultz, M.G., Schulz, M., Venkataraman, C., Zhang, H., Zhang, S., Bellouin, N., Guttikunda, S.K., Hopke, P.K., Jacobson, M.Z., Kaiser, J.W., Klimont, Z., Lohmann, U., Schwarz, J.P., Shindell, D., Storelvmo, T., Warren, S.G., Zender, C.S., 2013. Bounding the role of black carbon in the climate system: a scientific assessment. J. Geophys. Res. Atmos. 118, 5380–5552. https://doi.org/10.1002/jgrd.50171.

Buchholz, B., Fallon, S., Zermeño, P., Bench, G., Schichtel, B., 2013. Anomalous elevated radiocarbon measurements of $PM_{2.5}$. Nucl. Instrum. Methods Phys. Res., Sect. B 294, 631–635. https://doi.org/10.1016/j.nimb.2012.05.021.

Chang, Y., Liu, X., Deng, C., Dore, A.J., Zhuang, G., 2016. Source apportionment of atmospheric ammonia before, during, and after the 2014 APEC summit in Beijing using stable nitrogen isotope signatures. Atmos. Chem. Phys. 16, 11635–11647. https://doi.org/10.5194/acp-16-11635-2016.

Chen, B., Andersson, A., Lee, M., Kirillova, E.N., Xiao, Q., Kruså, M., Shi, M., Hu, K., Lu, Z., Streets, D.G., Du, K., Gustafsson, O., 2013. Source forensics of black carbon aerosols from China. Environ. Sci. Technol. 47, 9102–9108. https://doi.org/10.1021/es401599r.

Chen, J., Li, C., Ristovski, Z., Milic, A., Gu, Y., Islam, M.S., Wang, S., Hao, J., Zhang, H., He, C., Guo, H., Fu, H., Miljevic, B., Morawska, L., Thai, P., Lam, Y.F., Pereira, G., Ding, A., Huang, X., Dumka, U.C., 2017. A review of biomass burning: emissions and impacts on air quality, health and climate in China. Sci. Total Environ. 579, 1000–1034. https://doi.org/10.1016/j.scitotenv.2016.11.025.

Du, Z., He, K., Cheng, Y., Duan, F., Ma, Y., Liu, J., Zhang, X., Zheng, M., Weber, R., 2014. A yearlong study of water-soluble organic carbon in Beijing I: sources and its primary vs. secondary nature. Atmos. Environ. 92, 514–521. https://doi.org/10.1016/j.atmosenv.2014.04.060.

Dusek, U., Hitzenberger, R., Kasper-Giebl, A., Kistler, M., Meijer, H.A.J., Szidat, S., Wacker, L., Holzinger, R., Röckmann, T., 2017. Sources and formation mechanisms of carbonaceous aerosol at a regional background site in the Netherlands: insights from a year-long radiocarbon study. Atmos. Chem. Phys. 17, 3233–3251. https://doi.org/10.5194/acp-17-3233-2017.

Felix, J.D., Elliott, E.M., 2014. Isotopic composition of passively collected nitrogen dioxide emissions: vehicle, soil and livestock source signatures. Atmos. Environ. 92, 359–366. https://doi.org/10.1016/j.atmosenv.2014.04.005.

Felix, J.D., Elliott, E.M., Shaw, S.L., 2012. Nitrogen isotopic composition of coal-fired power plant NO_x: influence of emission controls and implications for global emission inventories. Environ. Sci. Technol. 46, 3528–3535. https://doi.org/10.1021/es203355v.

Felix, D.J., Elliott, E.M., Gish, T.J., McConnell, L.L., Shaw, S.L., 2013. Characterizing the isotopic composition of atmospheric ammonia emission sources using passive samplers and a combined oxidation-bacterial denitrifier approach. Rapid Commun. Mass Spectrom. 27, 2239–2246. https://doi.org/10.1002/rcm.6679.

Fisseha, R., Spahn, H., Wegener, R., Hohaus, T., Brasse, G., Wissel, H., Tillmann, R., Wahner, A., Koppmann, R., Kiendler-Scharr, A., 2009. Stable carbon isotope composition of secondary organic aerosol from β-pinene oxidation. J. Geophys. Res. 114, D02304. https://doi.org/10.1029/2008JD011326.

Freyer, H.D., 1991. Seasonal variation of $^{15}N/^{14}N$ ratios in atmospheric nitrate species. Tellus B 43, 30–44. https://doi.org/10.1034/j.1600-0889.1991.00003.x.

Gil, J., Lee, M., Han, J., Kim, S., Guenther, A., Kim, H., Kim, S., Park, H., 2018. Peroxyacetyl nitrate and ozone enhancement at Taehwa Research Forest under the influence of Seoul Metropolitan Area. Aerosol Air Qual. Res. 18, 2262–2273. https://doi.org/10.4209/aaqr.2017.11.0451.

Graven, H.D., 2015. Impact of fossil fuel emissions on atmospheric radiocarbon and various applications of radiocarbon over this century. Proc. Natl. Acad. Sci. U. S. A. 112, 9542–9545. https://doi.org/10.1073/pnas.1504467112.

Ham, J., Lee, M., Kim, H.S., Park, H., Cho, G., Park, J., 2016. Variation of OC and EC in $PM_{2.5}$ at Mt. Taehwa. J. Korea. Soc. Atmos. Environ. 32, 21–31.

Heal, M.R., 2014. The application of carbon-14 analyses to the source apportionment of atmospheric carbonaceous particulate matter: a review. Anal. Bioanal. Chem. 406, 81–98. https://doi.org/10.1007/s00216-013-7404-1.

Heaton, T.H.E., 1987. The $^{15}N/^{14}N$ ratios of plants in South Africa and Namibia: relationship to climate and coastal/saline environments. Oecologia 74, 236–246. https://doi.org/10.1007/BF00379365.

Heaton, T.H.E., 1990. $^{15}N/^{14}N$ ratios of NO_x from vehicle engines and coal-fired power stations. Tellus B 42, 304–307. https://doi.org/10.1034/j.1600-0889.1990.00007.x-i1.

Heaton, T.H.E., Spiro, B., Robertson, S.M.C., 1997. Potential canopy influences on the isotopic composition of nitrogen and sulphur in atmospheric deposition. Oecologia 109, 600–607. https://doi.org/10.1007/s004420050122.

Jimenez, J.L., Canagaratna, M.R., Donahue, N.M., Prevot, A.S.H., Zhang, Q., Kroll, J.H., Decarlo, P.F., Allan, J.D., Coe, H., Ng, N.L., Aiken, A.C., Docherty, K.S., Ulbrich, I.M., Grieshop, A.P., Robinson, A.L., Duplissy, J., Smith, J.D., Wilson, K.R., Lanz, V.A., Hueglin, C., Sun, Y.L., Tian, J., Laaksonen, A., Raatikainen, T., Rautiainen, J., Vaattovaara, P., Ehn, M., Kulmala, M., Tomlinson, J.M., Collins, D.R., Cubison, M.J., Dunlea, J., Huffman, J.A., Onasch, T.B., Alfarra, M.R., Williams, P.I., Bower, K., Kondo, Y., Schneider, J., Drewnick, F., Borrmann, S., Weimer, S., Demerjian, K., Salcedo, D., Cottrell, L., Griffin, R., Takami, A., Miyoshi, T., Hatakeyama, S., Shimono, A., Sun, J.Y., Zhang, Y.M., Dzepina, K., Kimmel, J.R., Sueper, D., Jayne, J.T., Herndon, S.C., Trimborn, A.M., Williams, L.R., Wood, E.C., Middlebrook, A.M., Kolb, C.E., Baltensperger, U., Worsnop, D.R., 2009. Evolution of organic aerosols in the atmosphere. Science 326 (80), 1525–1529. https://doi.org/10.1126/science.1180353.

Jung, J., Kawamura, K., 2011. Springtime carbon emission episodes at the Gosan background site revealed by total carbon, stable carbon isotopic composition, and thermal characteristics of carbonaceous particles. Atmos. Chem. Phys. 11, 10911–10928. https://doi.org/10.5194/acp-11-10911-2011.

Kanakidou, M., Seinfeld, J.H., Pandis, S.N., Barnes, I., Dentener, F.J., Facchini, M.C., Van Dingenen, R., Ervens, B., Nenes, A., Nielsen, C.J., Swietlicki, E., Putaud, J.P., Balkanski, Y., Fuzzi, S., Horth, J., Moortgat, G.K., Winterhalter, R., Myhre, C.E.L., Tsigaridis, K., Vignati, E., Stephanou, E.G., Wilson, J., 2005. Organic aerosol and global climate modelling: a review. Atmos. Chem. Phys. 5, 1053–1123. https://doi.org/10.5194/acp-5-1053-2005.

Kawamura, K., Kobayashi, M., Tsubonuma, N., Mochida, M., Watanabe, T., Lee, M., 2004. Organic and inorganic compositions of marine aerosols from East Asia: seasonal variations of water-soluble dicarboxylic acids, major ions, total carbon and nitrogen, and stable C and N isotopic composition. Geochem. Soc. Spec. Publ. 9, 243–265. https://doi.org/10.1016/S1873-9881(04)80019-1.

Kawano, K., Komatsu, N., 2012. Fire analysis of the Russian Far East in the passed seven years. 2012 IEEE International Geoscience and Remote Sensing Symposium, pp. 5939–5942 https://doi.org/10.1109/IGARSS.2012.6352256.

Kawashima, H., Kurahashi, T., 2011. Inorganic ion and nitrogen isotopic compositions of atmospheric aerosols at Yurihonjo, Japan: implications for nitrogen sources. Atmos. Environ. 45, 6309–6316. https://doi.org/10.1016/J.ATMOSENV.2011.08.057.

Kim, J., Yoon, S.-C., Jefferson, A., Zahorowski, W., Kang, C.-H., 2005. Air mass characterization and source region analysis for the Gosan super-site, Korea, during the ACE-Asia 2001 field campaign. Atmos. Environ. 39, 6513–6523. https://doi.org/10.1016/j.atmosenv.2005.07.021.

Kim, S.-W., Yoon, S.-C., Kim, J., Kim, S.-Y., 2007. Seasonal and monthly variations of columnar aerosol optical properties over east Asia determined from multi-year MODIS, LIDAR, and AERONET sun/sky radiometer measurements. Atmos. Environ. 41, 1634–1651. https://doi.org/10.1016/j.atmosenv.2006.10.044.

Kim, S., Kim, S.-Y., Lee, M., Shim, H., Wolfe, G.M., Guenther, A.B., He, A., Hong, Y., Han, J., 2015a. Impact of isoprene and HONO chemistry on ozone and OVOC formation in a semirural South Korean forest. Atmos. Chem. Phys. 15, 4357–4371. https://doi.org/10.5194/acp-15-4357-2015.

Kim, H., Lee, M., Kim, S., Guenther, A.B., Park, J., Cho, G., Kim, H.S., 2015b. Measurements of isoprene and monoterpenes at Mt. Taehwa and estimation of their emissions. Agric. For. Meteorol. 17, 217–226. https://doi.org/10.5532/KJAFM.2015.17.3.217.

Kirillova, E.N., Andersson, A., Han, J., Lee, M., Gustafsson, Ö., 2014. Sources and light absorption of water-soluble organic carbon aerosols in the outflow from northern China. Atmos. Chem. Phys. 14, 1413–1422. https://doi.org/10.5194/acp-14-1413-2014.

Kundu, S., Kawamura, K., 2014. Seasonal variations of stable carbon isotopic composition of bulk aerosol carbon from Gosan site, Jeju Island in the East China Sea. Atmos. Environ. 94, 316–322. https://doi.org/10.1016/j.atmosenv.2014.05.045.

Kundu, S., Kawamura, K., Lee, M., 2010. Seasonal variation of the concentrations of nitrogenous species and their nitrogen isotopic ratios in aerosols at Gosan, Jeju Island: implications for atmospheric processing and source changes of aerosols. J. Geophys. Res. 115, D20305. https://doi.org/10.1029/2009JD013323.

Kunwar, B., Kawamura, K., Zhu, C., 2016. Stable carbon and nitrogen isotopic compositions of ambient aerosols collected from Okinawa Island in the western North Pacific Rim, an outflow region of Asian dusts and pollutants. Atmos. Environ. 131, 243–253. https://doi.org/10.1016/J.ATMOSENV.2016.01.035.

Lee, M., Song, M., Moon, K.J., Han, J.S., Lee, G., Kim, K.-R., 2007. Origins and chemical characteristics of fine aerosols during the northeastern Asia regional experiment (Atmospheric Brown Cloud–East Asia Regional Experiment 2005). J. Geophys. Res. 112, D22S29. https://doi.org/10.1029/2006JD008210.

Lim, S., Lee, M., Lee, G., Kim, S., Yoon, S., Kang, K., 2012. Ionic and carbonaceous compositions of PM_{10}, $PM_{2.5}$ and $PM_{1.0}$ at Gosan ABC Superstation and their ratios as source signature. Atmos. Chem. Phys. 12, 2007–2024. https://doi.org/10.5194/acp-12-2007-2012.

Lim, S., Lee, M., Kim, S.-W., Yoon, S.-C., Lee, G., Lee, Y.J., 2014. Absorption and scattering properties of organic carbon versus sulfate dominant aerosols at Gosan climate observatory in Northeast Asia. Atmos. Chem. Phys. 14, 7781–7793. https://doi.org/10.5194/acp-14-7781-2014.

Mouteva, G.O., Fahrni, S.M., Santos, G.M., Randerson, J.T., Zhang, Y.-L., Szidat, S., Czimczik, C.I., 2015. Accuracy and precision of ^{14}C-based source apportionment of organic and elemental carbon in aerosols using the Swiss_4S protocol. Atmos. Meas. Tech. 8, 3729–3743. https://doi.org/10.5194/amt-8-3729-2015.

NIER, 2013. Studies on Effect of BVOCs on Ozone and Organic Aerosols (III). p. 1485011907.

NIER, 2014. Annual Report of Ambient Air Quality in Korea.

Pan, Y., Tian, S., Liu, D., Fang, Y., Zhu, X., Zhang, Q., Zheng, B., Michalski, G., Wang, Y., 2016. Fossil fuel combustion-related emissions dominate atmospheric Ammonia sources during severe haze episodes: evidence from ^{15}N-stable isotope in size-resolved aerosol ammonium. Environ. Sci. Technol. 50, 8049–8056. https://doi.org/10.1021/acs.est.6b00634.

Pan, Y., Tian, S., Zhao, Y., Zhang, L., Zhu, X., Gao, J., Huang, W., Zhou, Y., Song, Y., Zhang, Q., Wang, Y., 2018. Identifying ammonia hotspots in China using a national observation network. Environ. Sci. Technol. 52, 3926–3934. https://doi.org/10.1021/acs.est.7b05235.

Pavuluri, C.M., Kawamura, K., Swaminathan, T., 2015. Time-resolved distributions of bulk parameters, diacids, ketoacids and α-dicarbonyls and stable carbon and nitrogen isotope ratios of TC and TN in tropical Indian aerosols: influence of land/sea breeze and secondary processes. Atmos. Res. 153, 188–199. https://doi.org/10.1016/j.atmosres.2014.08.011.

Pöschl, U., 2005. Atmospheric aerosols: composition, transformation, climate and health effects. Angew. Chem. Int. Ed. 44, 7520–7540. https://doi.org/10.1002/anie.200501122.

Quinn, P.K., Charlson, R.J., Bates, T.S., 1988. Simultaneous observations of ammonia in the atmosphere and ocean. Nature 335, 336–338. https://doi.org/10.1038/335336a0.

Ramanathan, V., Carmichael, G., 2008. Global and regional climate changes due to black carbon. Nat. Geosci. 1, 221–227.

Santos, G.M., Moore, R.B., Southon, J.R., Griffin, S., Hinger, E., Zhang, D., 2007. AMS ^{14}C sample preparation at the KCCAMS/UCI Facility: status report and performance of small samples. Radiocarbon 49, 255–269. https://doi.org/10.1017/S0033822200042181.

Schleicher, N.J., Yu, Y., Cen, K., Chai, F., Chen, Y., Wang, S., Norra, S., 2013. Source identification and seasonal variations of carbonaceous aerosols in Beijing—a stable isotope approach. Urban Environment. Springer Netherlands, Dordrecht, pp. 263–270 https://doi.org/10.1007/978-94-007-7756-9_22.

Shang, X., Zhang, K., Meng, F., Wang, S., Lee, M., Suh, I., Kim, D., Jeon, K., Park, H., Wang, X., Zhao, Y., 2018. Characteristics and source apportionment of fine haze aerosol in Beijing during the winter of 2013. Atmos. Chem. Phys. 18, 2573–2584. https://doi.org/10.5194/acp-18-2573-2018.

Shilling, J.E., Zaveri, R.A., Fast, J.D., Kleinman, L., Alexander, M.L., Canagaratna, M.R., Fortner, E., Hubbe, J.M., Jayne, J.T., Sedlacek, A., Setyan, A., Springston, S., Worsnop,

D.R., Zhang, Q., 2013. Enhanced SOA formation from mixed anthropogenic and biogenic emissions during the CARES campaign. Atmos. Chem. Phys. 13, 2091–2113. https://doi.org/10.5194/acp-13-2091-2013.

Stein, A.F., Draxler, R.R., Rolph, G.D., Stunder, B.J.B., Cohen, M.D., Ngan, F., 2015. NOAA's HYSPLIT atmospheric transport and dispersion modeling system. Bull. Am. Meteorol. Soc. 96, 2059–2077. https://doi.org/10.1175/BAMS-D-14-00110.1.

Streets, D.G., 2003. An inventory of gaseous and primary aerosol emissions in Asia in the year 2000. J. Geophys. Res. 108, 8809. https://doi.org/10.1029/2002JD003093.

Streets, D.G., Yan, F., Chin, M., Diehl, T., Mahowald, N., Schultz, M., Wild, M., Wu, Y., Yu, C., 2009. Anthropogenic and natural contributions to regional trends in aerosol optical depth, 1980–2006. J. Geophys. Res. 114, D00D18. https://doi.org/10.1029/2008JD011624.

Trumbore, S., Gaudinski, J.B., Hanson, P.J., Southon, J.R., 2002. Quantifying ecosystem-atmosphere carbon exchange with a 14C label. Eos, Trans. AGU 83, 267–268. https://doi.org/10.1029/2002EO000187.

Turekian, V.C., Macko, S., Ballentine, D., Swap, R.J., Garstang, M., 1998. Causes of bulk carbon and nitrogen isotopic fractionations in the products of vegetation burns: laboratory studies. Chem. Geol. 152, 181–192. https://doi.org/10.1016/S0009-2541(98)00105-3.

Walters, W.W., Goodwin, S.R., Michalski, G., 2015. Nitrogen stable isotope composition ($\delta^{15}N$) of vehicle-emitted NO_x. Environ. Sci. Technol. 49, 2278–2285. https://doi.org/10.1021/es505580v.

Wang, Y., McElroy, M.B., Martin, R.V., Streets, D.G., Zhang, Q., Fu, T.-M., 2007. Seasonal variability of NO_x emissions over east China constrained by satellite observations: implications for combustion and microbial sources. J. Geophys. Res. 112, D06301. https://doi.org/10.1029/2006JD007538.

Wang, Y.-L., Liu, X.-Y., Song, W., Yang, W., Han, B., Dou, X.-Y., Zhao, X.-D., Song, Z.-L., Liu, C.-Q., Bai, Z.-P., 2017. Source appointment of nitrogen in $PM_{2.5}$ based on bulk $\delta^{15}N$ signatures and a Bayesian isotope mixing model. Tellus Ser. B Chem. Phys. Meteorol. 69, 1299672. https://doi.org/10.1080/16000889.2017.1299672.

Weber, R.J., Sullivan, A.P., Peltier, R.E., Russell, A., Yan, B., Zheng, M., de Gouw, J., Warneke, C., Brock, C., Holloway, J.S., Atlas, E.L., Edgerton, E., 2007. A study of secondary organic aerosol formation in the anthropogenic-influenced southeastern United States. J. Geophys. Res. Atmos. 112. https://doi.org/10.1029/2007JD008408 (n/a–n/a).

Widory, D., 2006. Combustibles, fuels and their combustion products: a view through carbon isotopes. Combust. Theor. Model. 10, 831–841. https://doi.org/10.1080/13647830600720264.

Widory, D., 2007. Nitrogen isotopes: tracers of origin and processes affecting PM_{10} in the atmosphere of Paris. Atmos. Environ. 41, 2382–2390. https://doi.org/10.1016/j.atmosenv.2006.11.009.

Widory, D., Roy, S., Le Moullec, Y., Goupil, G., Cocherie, A., Guerrot, C., 2004. The origin of atmospheric particles in Paris: a view through carbon and lead isotopes. Atmos. Environ. 38, 953–961. https://doi.org/10.1016/j.atmosenv.2003.11.001.

Xu, X., Trumbore, S.E., Zheng, S., Southon, J.R., McDuffee, K.E., Luttgen, M., Liu, J.C., 2007. Modifying a sealed tube zinc reduction method for preparation of AMS graphite targets: reducing background and attaining high precision. Nucl. Instrum. Methods Phys. Res., Sect. B 259, 320–329. https://doi.org/10.1016/J.NIMB.2007.01.175.

Yang, F., Chen, H., Du, J., Yang, X., Gao, S., Chen, J., Geng, F., 2012. Evolution of the mixing state of fine aerosols during haze events in Shanghai. Atmos. Res. 104–105, 193–201. https://doi.org/10.1016/j.atmosres.2011.10.005.

Ye, B., 2003. Concentration and chemical composition of $PM_{2.5}$ in Shanghai for a 1-year period. Atmos. Environ. 37, 499–510. https://doi.org/10.1016/S1352-2310(02)00918-4.

Yeatman, S.G., Spokes, L.J., Dennis, P.F., Jickells, T.D., 2001. Comparisons of aerosol nitrogen isotopic composition at two polluted coastal sites. Atmos. Environ. 35, 1307–1320. https://doi.org/10.1016/S1352-2310(00)00408-8.

Ying, Q., Cureño, I.V., Chen, G., Ali, S., Zhang, H., Malloy, M., Bravo, H.A., Sosa, R., 2014. Impacts of Stabilized Criegee Intermediates, surface uptake processes and higher aromatic secondary organic aerosol yields on predicted $PM_{2.5}$ concentrations in the Mexico City Metropolitan Zone. Atmos. Environ. 94, 438–447. https://doi.org/10.1016/j.atmosenv.2014.05.056.

Zhang, Y.L., Perron, N., Ciobanu, V.G., Zotter, P., Minguillón, M.C., Wacker, L., Prévôt, A.S.H., Baltensperger, U., Szidat, S., 2012. On the isolation of OC and EC and the optimal strategy of radiocarbon-based source apportionment of carbonaceous aerosols. Atmos. Chem. Phys. 12, 10841–10856. https://doi.org/10.5194/acp-12-10841-2012.

Zhang, Y.-L., Huang, R.-J., El Haddad, I., Ho, K.-F., Cao, J.-J., Han, Y., Zotter, P., Bozzetti, C., Daellenbach, K.R., Canonaco, F., Slowik, J.G., Salazar, G., Schwikowski, M., Schnelle-Kreis, J., Abbaszade, G., Zimmermann, R., Baltensperger, U., Prévôt, A.S.H., Szidat, S., 2015a. Fossil vs. non-fossil sources of fine carbonaceous aerosols in four Chinese cities during the extreme winter haze episode of 2013. Atmos. Chem. Phys. 15, 1299–1312. https://doi.org/10.5194/acp-15-1299-2015.

Zhang, Y.-L., Schnelle-Kreis, J., Abbaszade, G., Zimmermann, R., Zotter, P., Shen, R., Schäfer, K., Shao, L., Prévôt, A.S.H., Szidat, S., 2015b. Source apportionment of elemental carbon in Beijing, China: insights from radiocarbon and organic marker measurements. Environ. Sci. Technol. 49, 8408–8415. https://doi.org/10.1021/acs.est.5b01944.

Zhang, Y.-L., Kawamura, K., Agrios, K., Lee, M., Salazar, G., Szidat, S., 2016. Fossil and nonfossil sources of organic and elemental carbon aerosols in the outflow from Northeast China. Environ. Sci. Technol. 50, 6284–6292. https://doi.org/10.1021/acs.est.6b00351.

Zhao, P.S., Dong, F., He, D., Zhao, X.J., Zhang, X.L., Zhang, W.Z., Yao, Q., Liu, H.Y., 2013. Characteristics of concentrations and chemical compositions for $PM_{2.5}$ in the region of Beijing, Tianjin, and Hebei, China. Atmos. Chem. Phys. 13, 4631–4644. https://doi.org/10.5194/acp-13-4631-2013.